THE ASTROPHYSICAL JOURNAL, 409:139–148, 1993 May 20

MULTIFREQUENCY OBSERVATIONS OF THE OPTICALLY ACTIVE RADIO-QUIET QUASAR GQ COMAE II. ULTRAVIOLET, OPTICAL, AND INFRARED CONTINUUM VARIABILITY

MICHAEL L. SITKO[1,2,3,4,5]
Department of Physics, University of Cincinnati, OH 45221
ANNAMARIA K. SITKO[1,2]
Cincinnati Observatory, University of Cincinnati, Cincinnati, OH 45221
ANETA SIEMIGINOWSKA
Nicolaus Copernicus Astronomical Center, Bartycka 18, 00-716 Warsaw, Poland; and Harvard-Smithsonian Center for Astrophysics
AND
R. SZCZERBA
Nicolaus Copernicus Astronomical Center, Bartycka 18, 00-716 Warsaw, Poland
Received 1992 June 10; accepted 1992 November 5

ABSTRACT

This paper summarizes the data and preliminary results of a 3 yr long project to monitor the continuum variability of GQ Comae (PG 1202+281) from 0.12 μm to 3.5 μm. Substantial variability in the optical/ultraviolet flux was observed. The variability is examined using a geometrically thin accretion disk model. The model is able to reproduce the variations, but contains problems with physical consistency. A comparison of the optical/ultraviolet data and the infrared data indicates that the flux at 2.2 μm did not respond to the optical-ultraviolet continuum increase until nearly 250 days after the outburst and suggests that the variable flux at this wavelength is due to heated dust. We model the infrared emission with a dust component which is heated by the radiation from the accretion disk. We show that a simple model using a disklike distribution of heated dust grains can explain most of the infrared variability in a natural way.

Subject headings: dust, extinction — galaxies: photometry — infrared: galaxies — quasars: individual (GQ Comae) — ultraviolet: galaxies

1. INTRODUCTION

Variability studies of QSOs provide a powerful way to understand the physical nature and spatial relationships among the various emitting regions in those objects. Any successful model of the continuum radiation in active galactic nuclei (AGNs) will not only have to be able to explain the overall spectral energy distributions of these objects, but also to be able to explain the manner in which they are seen to vary. Thus more stringent constraints can be placed on the model parameters than can fits to a single observation.

It has been suggested that most of the optical/ultraviolet continuum emission is produced by an accretion disk. Malkan (1983), Sun & Malkan (1989), and Laor (1990) have achieved reasonable fits to individual "snapshots" of AGN spectra using models of geometrically thin, optically thick accretion disks. There is, however, considerable freedom in the range of parameters allowed, particularly since one can trade off the value of one parameter for another to achieve the same fit (Sitko 1986; Sun & Malkan 1989). Also, for high accretion rates the standard "α" models (Shakura & Sunyaev 1973) must include the contribution from electron scattering (Czerny & Elvis 1987) to the opacity when calculating spectra.

There is also great uncertainty about the nature of the infrared continuum emission in AGNs. Mentally extrapolating from the radio part of the spectrum, many early investigators simply assumed that the IR was dominated by synchrotron emission. However, the substantial polarization seen in the radio is not seen in the IR (Sitko & Zhu 1991). Furthermore, very acceptable fits of the IR spectrum can be made using models that have the IR dominated by heated dust (Barvainis 1987, 1990). Dust models predict that since the dust is located far enough from the central source for the grains to be below their evaporation temperatures, there ought to be a substantial time delay between any variability in the primary heating source (again, the optical/UVcontinuum) and the IR. Such a delay was reported for III Zw 2 by Lebofsky & Rieke (1980), who showed that the delay was consistent with heated dust. Rees et al. (1969) suggested that $t_{\rm var} \propto \lambda^{2.5}$ for typical dust parameters, so that the time delay observed ought to be longer for longer wavelengths. On the other hand, if the IR were due to synchrotron emission in a region whose magnetic field were in any way coupled to the central engine, the IR would be expected to respond immediately. In the models of Edelson & Malkan (1986), the IR-emitting synchrotron source sizes derived from spectral fitting are on the order of a light-day or less.

GQ Comae (PG 1202+281, $z = 0.165$) is a radio-quiet QSO with substantial optical/ultraviolet variability. Because of this,

[1] Guest Observer with the *International Ultraviolet Explorer* satellite, which is operated by the National Aeronautics and Space Administration, by the Science and Engineering Council of the United Kingdom, and by the European Space Agency.
[2] Visiting Astronomer at the Mount Lemmon Observing Facility, operated by the University of Minnesota and the University of California at San Diego.
[3] Visiting Astronomer at the Steward Observatory, operated by the University of Arizona.
[4] Visiting Astronomer, Kitt Peak National Observatory, National Optical Astronomy Observatories, operated by the Associated Universities for Research in Astronomy. Inc., under contract with the National Science Foundation.
[5] Visiting Astronomer at the Infrared Telescope Facility, which is operated by the University of Hawaii under contract to the National Aeronautics and Space Administration.

it is an ideal object for studying the physical nature of the optical/ultraviolet emitting region, and the spatial relationship of the infrared-emitting region to the optical/UV region. A series of ultraviolet (*IUE*) spectra with contemporaneous optical and infrared photometry (0.33 μm to 3.5 μm) over a 3 yr time span was obtained in order to determine the structure of the emitting regions in GQ Com. GQ Com is one of the most strongly and rapidly varying radio-quiet QSOs (the reason it was chosen for this type of project), and although its variability time scale is longer than that of the lower luminosity Seyfert galaxy NGC 5548 ($t_{var} \approx 100$ days; Peterson et al. 1991), it might be dangerous to conclude that the fairly large and rapid variability of GQ Com is entirely representative of objects in its class. In this paper, we discuss the continuum observations and crude theoretical models used to explain them. More sophisticated models are under development and will be discussed in a future paper. The results relating to the line emission variability are reported elsewhere (Sitko 1990).

2. OBSERVATIONS

2.1. *Ultraviolet Observations*

The UV observations were obtained with the *IUE* satellite, comprising 18 SWP, 1 LWR, and 1 LWP exposures, beginning in 1983 and extending into 1987. All of the observations were made with the large entrance aperture. The spectra were extracted with the GEX (Gaussian EXtraction) routine, and the standard flux calibration was applied. A complete description of the procedures used have already been reported (Sitko 1990). Table 1 lists the image number, UT date, Julian Day, luminosity at one representative wavelength (near 1365 Å) in the source frame, and the probable error of the luminosity.

2.2. *Optical and Infrared Photometry*

Optical and infrared photometric data were obtained during numerous observing runs between 1980 and 1987. The data prior to 1984 November are rather sporadic. Beginning in 1984 November, GQ Com was extensively monitored.

TABLE 1

ULTRAVIOLET CONTINUUM LUMINOSITIES[a]
LOG FLUX νL_ν (erg s^{-1})

Image Number	Date (UT)	JD[b]	Luminosity	Error
SWP 8900	81.04.04	4727.5	44.900	0.042
SWP 14049.....	83.01.21	5355.5	44.740	0.046
SWP 19721.....	83.04.14	5437.5	44.263	0.046
SWP 24580.....	84.11.30	6033.5	44.667	0.042
SWP 25257.....	85.02.16	6111.5	44.651	0.042
SWP 25551.....	85.03.30	6153.5	44.902	0.042
SWP 25798.....	85.04.28	6183.5	44.971	0.042
SWP 25933.....	85.05.14	6198.5	45.034	0.042
SWP 26411.....	85.07.13	6258.5	45.046	0.042
SWP 27166.....	85.11.23	6391.5	44.839	0.042
SWP 27710.....	86.02.13	6474.5	44.776	0.042
SWP 28033.....	86.03.26	6515.5	44.708	0.042
SWP 28346.....	86.05.20	6570.5	44.857	0.042
SWP 28604.....	86.07.04	6614.5	44.771	0.042
SWP 29781.....	86.11.30	6763.5	45.075	0.084
SWP 30237.....	87.02.02	6828.5	44.837	0.042
SWP 30679.....	87.04.01	6886.5	44.711	0.042
SWP 30870.....	87.04.26	6911.5	44.721	0.042
SWP 30958.....	87.05.12	6927.5	44.804	0.042

[a] Assumes $z = 0.165$, $H_0 = 75$ km s^{-1} Mpc^{-1}, and $q_0 = 0$, and a reddening correction of 0.035.
[b] Plus 2,440,000 days.

The bulk of the data was obtained at the KPNO 1.3 m telescope. For the majority of these observing runs, the Hermann InSb infrared photometer was used. On few occasions when Hermann was ill, his less-sensitive brother Otto was used. During most of these runs, the telescope was equipped with the Simulphote system for obtaining optical photometry the same night without an instrument change. Until late 1987 this system was manually operated, resulting in its being used only sporadically.

Some additional optical photometry was performed using the Two-Holer photopolarimeter on the 1.5 m telescope of the Mount Lemmon Observing Facility. The instrument and its operation are briefly described by Sitko, Schmidt, & Stein (1985).

The optical and infrared photometric data are listed in Table 2. The first column indicates the UT dates of the observations. Columns (2) through (10) are the magnitudes measured in the U(0.36 μm), B(0.44 μm), V(0.55 μm), R(0.64 μm), I(0.79 μm), J(1.25 μm), H(1.65 μm), K(2.25 μm), and L(3.5 μm) bands, respectively. Unless otherwise noted, the R and I data refer to the photometric system of Bessell (1976). A few observations were made on the R(0.7 μm) and I(0.9 μm) system of Johnson (1966) and are enclosed in square brackets. A few infrared points were also obtained at an effective wavelength of 3.75 μm (L') and are similarly indicated. For the infrared data, the error in the measurement is determined from photon statistics. The errors in the optical data are a combination of photon statistics and uncertainties in the extinction correction and transformation coefficients of the photometry reductions. The associated errors follow the value of the magnitude in Table 2 and are enclosed in parentheses. A few of the observations listed here were obtained by other observers (in one case as part of their own projects), are taken from an earlier paper (Sitko et al. 1982), or are taken from other sources in the literature. These additional sources of data are indicated in column (11).

2.3. *X-Ray and Far-IR Data*

Far-IR data were taken from the literature to aid in the modeling of the source. The three lowest frequency points are *IRAS* data from Impey & Neugebauer (1988). The next higher frequency point is from Landau et al. (1986). It is a statistically significant result, as opposed to the upper limit at the same frequency obtained by Impey & Neugebauer (1988, who also have placed GQ Com in a list of BL Lac objects and optically violent variable quasars [blazars], which is incorrect). The *Einstein* X-ray data are derived from Elvis et al. (1986).

2.4. *Fluxes and Luminosities*

All of the continuum observations that are illustrated in this paper have been converted into absolute fluxes and luminosities.

For the *IUE* data, the standard absolute flux calibrations as of 1986 were used (Holm et al. 1982; Cassatella & Harris 1983). The flux calibration for the optical data is that of Bessell (1979) for the observations on the Bessell system, and Hayes (1979) for the Johnson *RI* data. For the infrared data, the flux calibration used was that of Campins, Rieke, & Lebofsky (1985), except for the 3.75 μm data, where the calibration of Hayes (1979) was used.

The photometric and *IUE* data were corrected for interstellar reddening in the Milky Way using the reddening curve of Savage & Mathis (1979) for the optical and infrared data, and the mean cluster extinction of Massa & Fitzpatrick (1986)

TABLE 2

OPTICAL AND INFRARED MAGNITUDES

Date (UT) (1)	U (2)	B (3)	V (4)	R (5)	I (6)	J (7)	H (8)	K (9)	L (10)	Notes (11)
80.12.16.....	...	...	...	...	...	...	...	12.45 (0.09)	...	a
81.01.04.....	15.58 (0.03)	16.61 (0.03)	16.42 (0.03)	[15.99 (0.03)]	[15.15 (0.03)]	...	...	...	...	a
81.02.02.....	15.49 (0.03)	16.49 (0.03)	16.41 (0.03)	[15.82 (0.03)]	[15.16 (0.03)]	...	...	...	...	a
81.03.08.....	...	...	...	...	...	...	...	...	11.06 (0.03)	a
81.05.09.....	...	...	...	...	...	14.98 (0.22)	14.44 (0.10)	12.25 (0.06)	10.31 (0.32)	a
81.05.10.....	...	...	...	...	...	14.73 (0.14)	13.51 (0.08)	12.20 (0.03)	10.51 (0.24)	a
83.04.14.....	...	15.69 (0.02)	15.62 (0.01)	[15.26 (0.03)]	...	...	...	12.61 (0.08)	...	b
83.04.16.....	...	15.66 (0.02)	15.60 (0.01)	[15.28 (0.03)]	...	...	...	12.46 (0.05)	...	b
83.06.03.....	15.23 (0.05)	15.99 (0.04)	15.92 (0.06)	15.64 (0.07)	14.96 (0.08)	...	...	...	...	c
83.06.05.....	15.52 (0.14)	15.92 (0.09)	15.84 (0.10)	15.63 (0.09)	14.72 (0.11)	...	...	...	...	c
84.02.01.....	...	16.73 (0.05)	16.50 (0.05)	...	...	...	...	...	...	d
84.05.27.....	15.63 (0.04)	16.56 (0.04)	16.22 (0.05)	16.01 (0.06)	15.34 (0.07)	...	...	...	...	
84.05.28.....	15.73 (0.05)	16.58 (0.04)	16.32 (0.05)	15.97 (0.06)	15.18 (0.07)	...	...	...	...	
84.11.27.....	...	16.65 (0.06)	16.30 (0.06)	...	15.22 (0.06)	...	...	...	...	
84.11.28.....	...	16.66 (0.06)	16.29 (0.06)	...	15.24 (0.06)	...	...	...	...	
84.12.02.....	...	...	...	...	...	14.56 (0.20)	13.75 (0.10)	12.42 (0.06)	...	
85.01.10.....	...	...	16.50 (0.05)	...	...	...	...	...	...	d
85.02.14.....	...	16.63 (0.07)	16.41 (0.06)	16.12 (0.05)	...	14.77 (0.12)	13.80 (0.10)	12.70 (0.06)	10.74 (0.17)	
85.02.15.....	...	...	...	...	...	14.79 (0.24)	13.72 (0.16)	12.72 (0.12)	10.90 (0.19)	
85.02.26.....	...	...	16.27 (0.05)	...	...	...	...	...	...	d
85.03.22.....	15.39 (0.08)	16.38 (0.08)	16.34 (0.07)	15.82 (0.07)	15.23 (0.08)	14.63 (0.14)	13.97 (0.08)	12.89 (0.06)	10.55 (0.20)	
85.03.23.....	15.37 (0.05)	16.31 (0.05)	16.14 (0.04)	15.95 (0.04)	15.19 (0.05)	14.37 (0.14)	13.86 (0.11)	12.69 (0.05)	10.77 (0.22)	
85.03.24.....	15.39 (0.05)	16.35 (0.05)	16.21 (0.04)	15.89 (0.04)	15.33 (0.04)	14.64 (0.16)	13.70 (0.11)	12.52 (0.07)	10.40 (0.15)	
85.03.25.....	15.27 (0.03)	16.24 (0.03)	16.16 (0.03)	[15.72 (0.03)]	[15.16 (0.03)]	...	...	...	...	e
85.04.15.....	15.27 (0.03)	16.31 (0.03)	16.02 (0.03)	[15.78 (0.03)]	[15.18 (0.03)]	...	...	...	...	e
85.04.27.....	...	...	...	...	...	14.65 (0.15)	13.90 (0.15)	12.71 (0.09)	10.73 (0.32)	
85.04.30.....	...	...	15.93 (0.11)	...	...	...	...	...	...	
85.05.19.....	15.03 (0.05)	16.04 (0.05)	15.91 (0.05)	15.62 (0.05)	14.90 (0.06)	...	...	...	...	
85.05.21.....	14.89 (0.05)	16.04 (0.05)	15.91 (0.05)	15.85 (0.05)	15.03 (0.05)	...	...	...	...	
85.05.23.....	...	...	...	...	...	14.72 (0.13)	13.71 (0.10)	12.64 (0.07)	10.80 (0.56)	
85.05.24.....	...	...	...	...	...	14.42 (0.17)	13.94 (0.15)	12.52 (0.07)	10.60 (0.53)	
85.07.14.....	...	...	...	...	...	...	...	12.76 (0.04)	10.93 (0.03)	f
85.11.07.....	15.35 (0.05)	16.24 (0.04)	16.14 (0.04)	15.73 (0.05)	...	...	...	...	...	
85.11.15.....	...	...	...	...	...	14.14 (0.17)	13.58 (0.17)	12.52 (0.10)	...	
85.11.16.....	...	...	16.05 (0.06)	...	...	...	...	...	...	
85.11.18.....	...	...	...	...	...	...	...	12.45 (0.08)	10.49 (0.16)	
85.11.19.....	...	...	...	...	...	14.35 (0.15)	13.84 (0.16)	12.60 (0.09)	10.50 (0.26)	
85.12.19.....	15.32 (0.04)	16.24 (0.04)	16.02 (0.04)	15.59 (0.04)	...	...	...	...	...	
86.01.08.....	...	...	...	...	...	14.51 (0.10)	13.54 (0.05)	12.56 (0.06)	10.98 (0.16)	
86.01.09.....	15.50 (0.04)	16.40 (0.04)	16.06 (0.04)	15.70 (0.04)	15.03 (0.05)	...	...	...	...	
86.01.10.....	...	...	...	...	...	14.52 (0.11)	13.64 (0.08)	12.36 (0.06)	11.05 (0.18)	
86.02.15.....	15.30 (0.06)	16.28 (0.06)	16.12 (0.06)	15.70 (0.06)	14.92 (0.06)	...	...	...	...	g
86.03.15.....	...	...	...	...	...	14.37 (0.05)	13.56 (0.03)	12.44 (0.02)	10.93 (0.09)	
86.05.30.....	...	...	...	...	...	14.31 (0.08)	13.64 (0.04)	12.51 (0.05)	11.04 (0.33)	
86.06.13.....	15.60 (0.05)	16.47 (0.05)	16.18 (0.04)	15.81 (0.04)	15.20 (0.04)	...	...	...	...	
86.11.27.....	...	...	16.27 (0.09)	...	...	...	...	...	...	
86.11.28.....	...	...	16.04 (0.17)	...	...	14.40 (0.07)	13.65 (0.06)	12.58 (0.06)	10.85 (0.22)	
86.11.29.....	...	...	16.00 (0.04)	...	...	14.50 (0.10)	13.70 (0.06)	12.55 (0.04)	10.76 (0.18)	
86.12.01.....	15.51 (0.04)	16.48 (0.04)	16.04 (0.04)	15.65 (0.04)	...	...	...	...	10.93 (0.17)	
86.12.02.....	...	...	...	...	...	...	...	...	10.77 (0.24)	
87.02.18.....	15.27 (0.03)	16.18 (0.03)	16.03 (0.03)	15.69 (0.03)	15.04 (0.03)	...	...	...	...	
87.02.22.....	...	...	...	...	...	14.49 (0.06)	13.67. (0.04)	12.56 (0.03)	10.83 (0.08)	
87.02.23.....	...	...	...	...	...	14.46 (0.06)	13.61 (0.04)	12.60 (0.03)	10.81 (0.09)	
87.03.24.....	...	...	...	...	...	...	...	12.65 (0.01)	...	h
87.05.01.....	...	...	...	...	...	14.63 (0.06)	13.72 (0.06)	12.75 (0.04)	11.20 (0.27)	
87.05.02.....	15.38 (0.04)	16.40 (0.03)	16.24 (0.03)	15.91 (0.03)	15.24 (0.04)	...	13.64 (0.07)	12.71 (0.05)	10.91 (0.37)	
87.05.03.....	...	...	...	...	...	...	...	...	10.69 (0.15)	
87.05.04.....	15.39 (0.04)	16.43 (0.04)	16.19 (0.03)	15.88 (0.04)	15.24 (0.04)	14.81 (0.12)	13.83 (0.07)	12.89 (0.06)	10.77 (0.14)	
87.05.05.....	...	...	...	...	...	14.58 (0.11)	13.72 (0.07)	12.54 (0.06)	10.79 (0.19)	
87.11.13.....	15.01 (0.03)	15.72 (0.03)	15.82 (0.02)	15.60 (0.03)	15.02 (0.03)	...	13.77 (0.21)	12.36 (0.08)	...	
87.11.15.....	...	...	...	...	...	...	...	12.58 (0.06)	[10.56 (0.11)]	i
87.11.16.....	...	...	...	...	...	14.43 (0.16)	13.69 (0.10)	12.62 (0.07)	[10.90 (0.16)]	i
89.03.13.....	...	...	...	...	...	...	...	12.32 (0.02)	...	h

[a] Data are from Sitko et al. 1982.
[b] Data are from Landau et al. 1986.
[c] Small drift in instrument sensitivity during night.
[d] Observations made by W. Keel.
[e] Observations made by W. Z. Wisniewski.
[f] Observations made by R. Howell.
[g] Observations made by G. D. Schmidt; some thin currus in sky.
[h] Observation made at the Infrared Telescope Facility as part of another project (Sitko & Zhu 1991).
[i] Observations made at L' ($\lambda_{\rm eff} \approx 3.7\ \mu$m).

TABLE 3

OPTICAL POLARIMETRY

Date (UT)	Filter[a]	Q (%)	U (%)	σ (%)	P (%)	θ (°)
78.03.04[b]	W	0.28	−0.20	0.15	0.30 ± 0.15	162 ± 13
80.04.12[b]	W	0.76	−0.08	0.35	0.68 ± 0.35	177 ± 13
87.04.24	K	−0.50	−0.28	0.51	<1.4[c]	...
89.03.13	K	−0.21	−0.51	0.18	0.52 ± 0.18	124 ± 9
92.03.25	W	0.21	−0.35	0.15	0.38 ± 0.15	150 ± 10
92.03.26	W	0.56	0.09	0.18	0.54 ± 0.18	5 ± 10
Combined:.....	K	−0.24	−0.48	0.17	0.51 ± 0.17	122 ± 9
	W	0.35	−0.17	0.09	0.39 ± 0.09	167 ± 7

[a] W = optical white light (no filter); K = 2.2 μm filter.

[b] From Stockman, Moore, & Angel (1984). The percent polarization from their Table 1 has been corrected here for the positive bias in low signal-to-noise values.

[c] 95% confidence upper limit.

for the UV data. The value of $E(B-V)$ assumed was 0.01 mag, as determined from the maps of Burstein & Heiles (1982).

These absolute flux data were converted into luminosities in the source reference frame, using a redshift of $z = 0.165$, a Hubble parameter H_0 of 75 km s^{-1} Mpc^{-1}, and a deceleration parameter $q_0 = 0$.

The errors in the fluxes and luminosities of the IR and optical data were calculated from the observed errors of the magnitude values. For the *IUE* data, the errors were the combined errors of the fits in WBINS (the *IUE* routine that calibrates mean fluxes over a wavelength bin), plus an assumed 10% uncertainty in the detector gain of the instrument. For one image (SWP 29781), the continuum was difficult to determine, so the value of the error was doubled.

2.5. *Optical and Infrared Polarimetry*

Optical polarization measurements of GQ Com were made with the Two-Holer photopolarimeter on the Mount Bigalow 1.55 m telescope of the Steward Observatory. The instrument its operation is described by Sitko et al. (1985). The results are reported in Table 3. Earlier observations made by Stockman, Moore, & Angel (1984) are also included. Additional infrared measurements that were previously reported (Sitko & Zhu 1991) are also listed. Because of the positive bias that is always present in the calculated total polarization when the signal-to-noise is less than 4, we have reported the individual normalized Stokes parameters as well as the bias-corrected polarization. For those data with upper limits only, the 95% ($\approx 2\,\sigma$) upper limit to the data, as described by Simmons & Stewart (1985), is listed. For each wavelength band, we have also combined the Stokes parameters to derive a "best" value for the polarization, assuming no polarization variability.

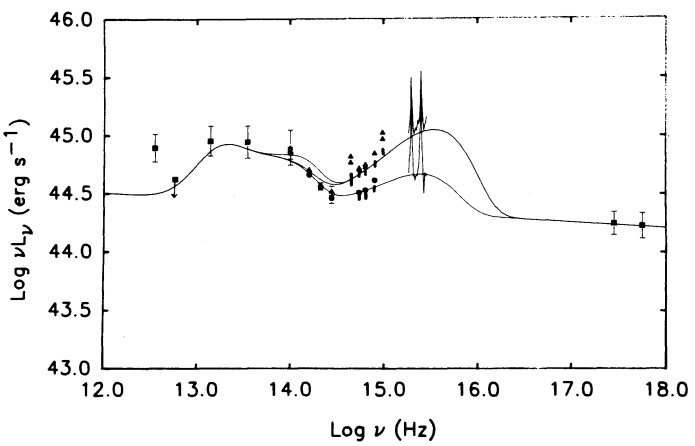

FIG. 1.—The variable emission of GQ Com. The infrared, optical, and ultraviolet (UVOIR) data were obtained during two different epochs, separated by 3 months. The far-IR and X-ray data are from the literature and are not simultaneous with either epoch of UVOIR data. The curves represent the emission predicted by the models in the text. The vertical lines beneath the *UBVRI* points are the result of correcting for emission line contamination in those bands and represent an estimate of the true continuum flux.

3. SUMMARY OF THE OBSERVATIONS

3.1. *UV-Optical Continuum Variability*

The data in this project were divided into 11 epochs. Each epoch consists of UV, optical, and IR data obtained, in general, within a few days of one another.

Figure 1 shows the range in monochromatic luminosity exhibited by GQ Com in the infrared, optical, and ultraviolet (UVOIR) for two epochs in time.

The effect of emission lines to the V, R, and I filters were determined using earlier spectra of GQ Com (Stoughton & Osterbrock 1980; Zheng et al. 1987) but are nonsimultaneous and so only approximate. Similarly, the U and B filters are contaminated by numerous emission line blends. The contribution of this emission was estimated using the published spectra and the models outlined below. The resulting corrected *UBVRI* data are also shown in the figure.

The luminosity of the source in the UV and optical, as a function of time, is shown in Figure 2. Soon after the intensive monitoring of the object began (in 1984 November), GQ Com underwent a major outburst in UVO luminosity, with the luminosity increasing by more than a factor of 2 in about 3 months.[6] The time scale of variability t_{var} in the UV (defined as $dt/d\ln L_\nu$ at 1400 Å in the object's rest frame) for this outburst was 100 days (with a minimum observed two-folding time of 50 days at the start of the outburst). The outburst was followed by a subsequent decline in the UV with $t_{var} \approx 300$–350 days. The decline in the V band is considerably longer and overlaps the next UV/optical rise. The UV and optical light curves were cross-correlated using the discrete correlation function (DCF) of Edelson & Krolik (1988). The DCF power is peaked at 0 ± 50 days, but there is a weak tail out to 300 days (the UV/V DCF is illustrated and discussed briefly in Appendix A). Both the light curves and their cross-correlation indicate that the

[6] The amplitude of the variability reported here differs from that of Fig. 2 of Sitko (1986) since that figure contains a factor of 2 error in its vertical scale.

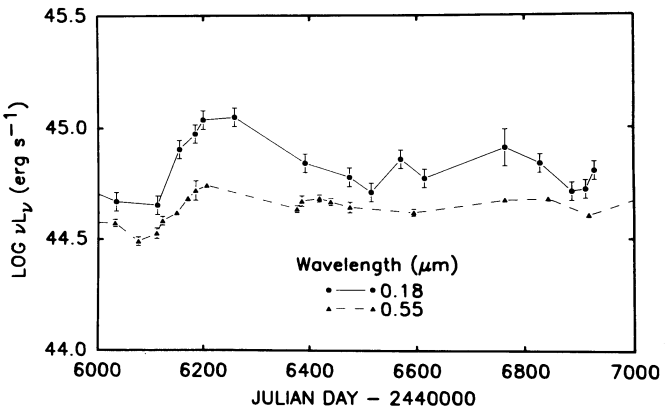

FIG. 2.—The light curve of GQ Com from 1985 November to 1987 May at 0.18 μm and 0.55 μm (observer's reference frame).

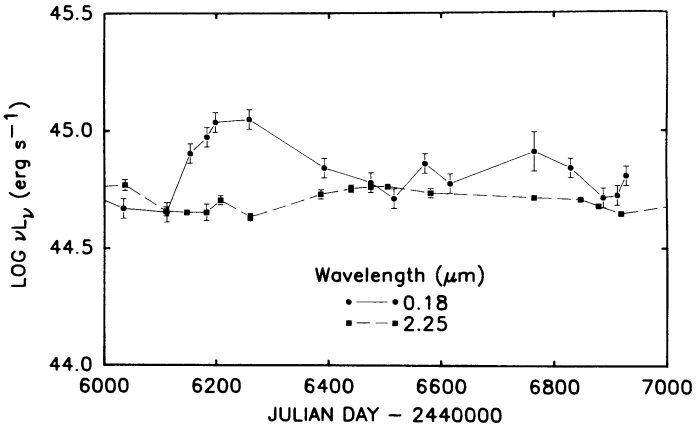

FIG. 3.—The light curve of GQ Com from 1985 November to 1987 May at 0.18 μm and 2.25 μm (observer's reference frame).

UV and optical luminosities increase with no substantial time delay (at least less than 50 days), but that the decline time of the optical exceeds that of the UV.

3.2. *Infrared Variability*

The UV and K-band light curves are shown together in Figure 3. It is evident from this plot that the IR seems to lag the UVO outburst. Assuming that the rise in the IR flux is related to the earlier rise in the UV flux, the time delay is approximately 250 days, easily seen as well in the UV/K cross-correlation plot in Appendix A (the peak at -200 days is the IR rise correlated with the next UV rise, which is assumed not to be causally related). The long time delay and low (less than 0.5%) 2.2 μm polarization (see below) indicate that the source of the IR emission is unlikely to be synchrotron radiation, but rather thermal radiation from heated dust grains. A similar delay time is seen in Fairall 9 (Clavel, Wamsteker, & Glass 1989).

If this interpretation is correct, we would expect that the IR response ought to be dependent on the wavelength observed for wavelengths greater than about 2.5 μm, where the emission comes from grains at different distances.[7] The grains closest to the heating source will dominate the shorter wavelengths and respond earlier to changes in the incident radiation. Figure 4 shows the light curves at 1.65 μm(H) and 2.25 μm(K). It is evident that the variation at 1.65 μm resembles that at 2.25 μm, although the amplitude is smaller at 1.65 μm. The UV/H cross-correlation is similar to that of UV/K (Appendix A), and although the power of the DCF at 100 days is higher at H than at K, it is only a 1.3 σ difference.

In Figure 5, the light curve at 3.5 μm (L) is plotted along with the UV and K light curves. The plot shows that there was a significant long-term rise in the 3.5 μm flux that seemed to be peaking out about 700 days after the UV outburst, and this time delay is also evident on the UV/L cross-correlation plot (Appendix A). The delay, if these K and L variations are due to dust emission, would be expected to occur roughly $(3.5/2.25)^{2.5} \times 250$ days = 750 days after the UV outburst and is therefore in agreement with the observations.

[7] The emission at shorter wavelengths is produced by the Wien tail of the very hottest and closest grains, whose emission peaks at 2 μm for grains with $T \approx 1800$ K. Since they are all near the inner edge of the dust zone, no dependence of time delay on wavelength is expected for wavelengths shorter than about 2.5 μm for similar-sized grains.

3.3. *Optical and Infrared Polarimetry*

The observed optical polarization is 0.51% $\pm$ 0.17%. Laor, Netzer, & Piran (1990) have investigated the polarization produced by scattering effects in disk models that include the effects of general relativity. In one model, they assume the disk radiates as an optically thick blackbody with a frequency-independent limb-darkening law. For this model, a 2% upper limit on the optical polarization constrains cos i (where i is the inclination angle of the disk axis to the line of sight) to be greater than about 0.7. In a second model, they calculate the polarization from a relativistic disk using a model atmosphere dominated by scattering using the Eddington approximation. In this second model, low optical polarization occurs at all but the lowest values of cos i, placing almost no constraints on the disk inclination.

The plane of polarization in the IR is similar to, but not identical with, that of the optical polarization. Only one really good IR point is available, however, and more data would be useful in deriving any definite conclusions about differences in the optical and IR polarization characteristics. Measurements of other "normal" QSOs suggest that the planes of optical and IR polarization are generally the same (Sitko & Zhu 1991) and also suggest that both arise from the same mechanism. Synchrotron emission is unlikely to contribute significantly to the IR emission, or the IR would probably have higher polariza-

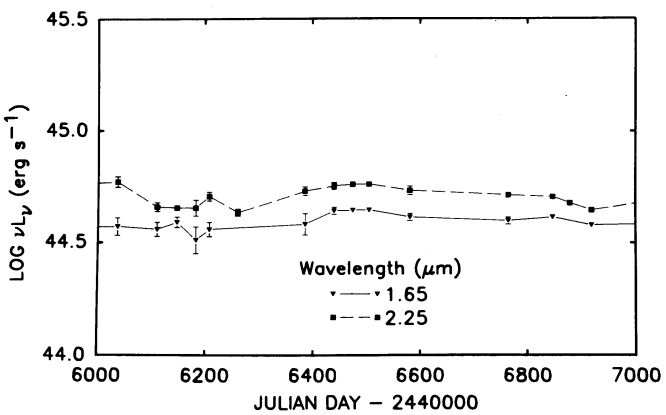

FIG. 4.—The light curve of GQ Com from 1985 November to 1987 May at 1.65 μm and 2.25 μm (observer's reference frame).

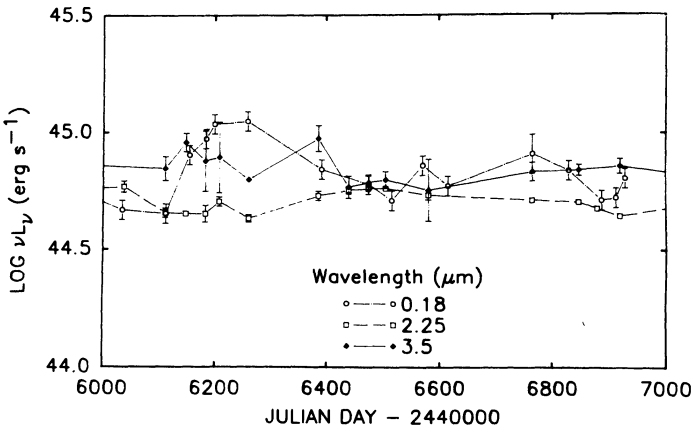

FIG. 5.—The light curve of GQ Com from 1985 November to 1987 May at 0.18 μm, 2.25 μm, and 3.5 μm (observer's reference frame).

tion. If the observed low polarization is due to scattering, then the scattering geometry that produces the IR polarization is like that which polarizes the optical light.

The similarity of the optical and IR polarizations in "normal" QSOs suggests that much of it is produced outside the accretion disk itself. If so, the intrinsic polarization of both the UVO and IR emission may be considerably less than the observed value. Whether this effectively constrains the inclination of the accretion disk depends on the assumed viscosity of the disk (Laor et al.).

4. UNIFIED MODEL OF THE CONTINUUM AND ITS VARIABILITY

4.1. *General Considerations*

We take as our starting point the hypothesis that the large UV flux component, the "Big Blue Bump," is produced by a geometrically thin, optically thick accretion disk. While there is still a great deal of controversy concerning the details of the accretion, it still forms a useful model that makes specific predictions which can be tested.

It is also evident from the preceding discussion that the IR variations are entirely consistent with the hypothesis that the IR emission, at least at wavelengths greater than 2 μm, are probably dominated by thermal emission of dust grains heated by the central radiation source. The time delays between the UV outburst and the K and L outbursts are just what is predicted for grains situated a large distance from the heating source, and whose minimum distance is determined by their evaporation temperature. The lower amplitude at H indicates that a significantly greater fraction of the flux there might not be due to dust, but could be due to the low-energy tail of the accretion disk or perhaps a third emission component. If the region containing the dust is the source of mass that powers the accretion disk, it is likely to have some angular momentum and some cylindrical symmetry.

Finally, in this model, a third component is assumed to be present at some level to be determined by the modeling. For simplicity, we take this to be a simple power law which provides the observed X-ray flux and much of the 1 μm flux, yet does not violate the observed 60 μm upper limit.

In summary, we model the continuum energy distribution with a composite model that consists of a central accretion disk, a dust disk, and a third additional source of flux whose spectrum was assumed to be a power law.

4.2. *General Characteristics of the Accretion Disk Model*

As a first approximation, we have investigated the nature of the UVO variability using the standard geometrically thin, optically thick accretion disk model. We have assumed that the disk radiates locally as a blackbody. General relativity affects are included after Novikov & Thorne (1973). The radial temperature gradient was determined from Page & Thorne (1974). Corrections for gravitational effects on the light transfer to the observer were taken from Cunningham (1975). Details of the modeling as applied to GQ Com are described more fully by Sitko (1986).

Since the probability that the disk is seen almost exactly face-on is slight, and if it is nearly equator-on and fed by a disk or torus with a similar geometry it will be obscured, we choose an intermediate inclination angle for the disk, with $\cos i = 0.75$ (in some accretion disk models the low observed optical polarization may also indicate a small inclination angle). As described earlier (Sitko 1986; Sun & Malkan 1989), the inclination angle and value for the central mass can be traded off to some extent.

Since we are assuming a rapidly rotating black hole as the central mass, the inner edge of the disk is $1.23R_G$ (where $R_G \equiv GM/c^2$). The outer extent of the disk was set by terminating the disk model at the point where it becomes unstable due to self-gravity (Goldreich & Lynden-Bell 1965; Sakimoto & Coroniti 1981). Here we have assumed that the contribution of the self-gravitating region of the disk to the observed flux is not signifcant. The total flux near $\log \nu = 14.5$ (near the J band) is most affected by changes in the outer disk limit (Bechtold et al. 1986). In our model, the disk contributes about 15% of the light in this band, so the contribution of the disk is not negligible, but it is also not large enough for us to place significant limits on the value of the outer radius nor on α. We should caution that the contribution to the flux could be greater in a different model.

4.3. *General Characteristics of the Dusty Disk Model*

The model used to reproduce the observed IR emission is similar to that of Barvainis (1987, 1990). It consists of a distribution of a chosen geometry, particle size, and radial particle density gradient. The particles intercept light from the central source, in this case the accretion disk, and reradiate the energy at longer wavelengths. The temperatures of the grains are determined by their distance from the central source, the optical depth due to grains closer to the source, and the grain sizes and compositions. Recently, Neugebauer et al. (1990) have measured the angular size of the Seyfert galaxy NGC 4151 at 11.3 μm. They found that the central infrared source with grains at $T \approx 200$ K has a radius of 5 pc. Since, for a given temperature, the distance of a grain scales as $L^{1/2}$ (where L is the luminosity), we would expect this region in GQ Com to be at about 80 pc ($L_{\rm GQCom}/L_{\rm NGC\,4151} \approx 300$) and that of Fairall 9 to be at about 40 pc. This suggests we consider a dust geometry which is still partly optically thin in the UV at distances larger than the dust region modeled by Barvainis (1992) for Fairall 9.

In this model the dust disk was assumed to have plane-parallel geometry with half thickness z, be seen face-on (for simplicity) with a biconical opening (with a certain solid angle covered), have an evacuated central cavity whose size ($R_{\rm in}$) is set by grain evaporation (temperature $T_{\rm ev}$), be made of carbonaceous (actually graphitic) grains of a certain size (A), have a certain inner density (n_l) and radial density distribution β [where $n(r) = n_l r^{-\beta}$], and have a minimum temperature ($T_{\rm min}$

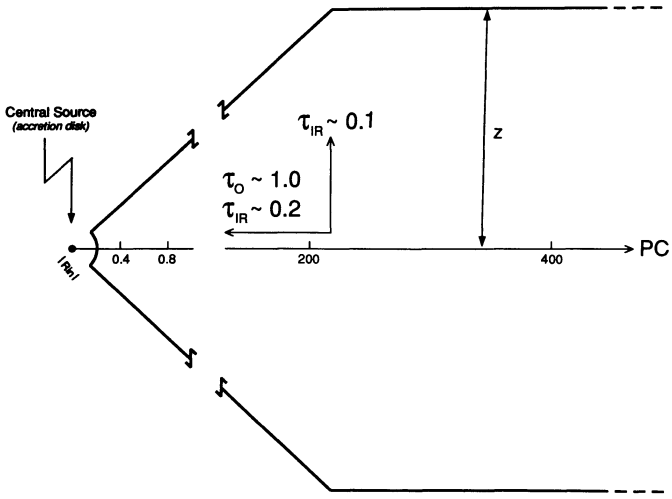

FIG. 6.—The geometry of the dust disk model, as described in the text. The innermost edge is set by the evaporation temperature of the grains. The opening angle was determined by recent estimates of the ratio of obscured to unobscured broad-line regions, assuming these correspond to Seyfert 2 and Seyfert 1 galaxies, respectively. The scale height of the dust was taken to be similar to that of the inner regions of the Milky Way. The optical depth to the central radiation source in the IR and optical, and normal to the disk in the IR, are also shown.

set to 20 K) in its outermost regions. The geometry of the disk is shown in Figure 6. The emission of the dust disk was determined by calculating the emission of the grains heated by the central accretion disk (which is seen by the dusty disk at a greater inclination angle). The rationale for assuming this type of model will be outlined.

Recent unified models of AGN's suggest that they consist of a central source surrounded by an obscuring torus of material. In the Milky Way, the warm dust has a scale height on the order of 1 pc in the innermost region (Genzel & Townes 1987 and sources therein), while it increases to about 100 pc farther out, scaling roughly with the molecular cloud height (Combes 1991 and sources therein). The dust disk presumably has a roughly biconical opening, allowing some fraction of the central source to be seen unobscured. It is believed that many Seyfert 2 galaxies may simply be obscured Seyfert 1 objects, like NGC 1068 (Antonucci & Miller 1985) and other Seyfert 2 galaxies (Tran, Miller, & Kay 1992). If this is the case, then the mean opening angle of the torus as seen by the central object should be related to the relative numbers of Seyfert 2 to Seyfert 1 galaxies. While the observed rato is near unity, a consideration of selection effects could push this ratio up much higher. The opening angle chosen here assumes that all Seyfert 2 galaxies are obscured Seyfert 1 galaxies, and the ratio of obscured to unobscured is 4 to 1, as suggested by Osterbrock & Shaw (1988).

For simplicity, the grains were chosen to be graphite with a single size. The grain size, innermost density and radial density distribution, and evaporation temperature were left to be determined by the model fits. However, the evaporation temperature for graphite is approximately 1800 K, and the gas densities in the inner Milky Way molecular clouds are $\sim 10^3$ cm^{-3}, which corresponds to a grain number density $\sim 5 \times 10^{-10}$ cm^{-3} for a gas/dust ratio of 100, and 0.15 μm graphite grains (mass density ~ 2.2 g cm^{-3}). The minimum density and temperature were set to equal the Galactic plane values in the Milky Way in the vicinity of the Sun.

4.4. *The Third Component*

Finally, the presence of significant 1 μm emission indicates that at least one other emission process is operating. If this spectral component is a power law, and it extends from the far-IR to the X-rays, then its characteristics can be constrained by the observed X-ray flux and 1 and 60 μm flux limits. We use this to find an upper limit on any synchrotron or optically thin free-free source present. The low polarization (both optical and infrared) suggests that this component is probably not synchrotron emission, unless the magnetic field structure is highly nonuniform, or the polarization is destroyed by Faraday effects (Sitko 1988).

4.5. *Fits to the Observations*

Figure 1 showed data from two epochs, centered around 1985 February 15 (filled circles and lower UV spectrum) and 1985 May 19 (filled triangles and upper UV spectrum). Also shown are the results of our model. The central black hole mass is $3 \times 10^8\ M_\odot$. The only parameter allowed to vary in the figure is the accretion rate which goes from 0.04 $M_\odot$ yr^{-1} to 0.15 $M_\odot$ yr^{-1}. The following dusty disk model parameters apply: $z = 200$ pc, $SA = 0.8 \times 4\pi$ sr, $T_{\rm min} = 20$ K, $T_{\rm ev} = 1700$ K, $A = 0.15$ μm, $n_l = 2 \times 10^{-10}$ cm^{-3}, and $\beta = 1.0$.

With these parameters, the optical depth at 2 μm never exceeds 0.1 when looking normal to the dust plane, so the dust disk is optically thin in the IR and radiative transfer effects are minor. The optical depth to the UVO source is zero within 45° of the disk axis, jumps to 1.0 at the edge of the opening, and reaches 2.0 when viewed 75° from the disk axis.

The temperature of the grains is determined by the size and composition. Here we assume graphite grains whose emissivity is given by Draine & Lee (1984), whose equilibrium temperature will be (for grain sizes close to 0.05 μm)

$$T_{\rm gr} = 1600[L_{\rm UVO,46}/r_{\rm pc}^2]^{1/5.6} e^{-\tau/5.6} [0.05/A_{\mu\rm m}]^{1/5.6} \text{ K} , \quad (1)$$

where $L_{\rm UVO,46}$ is the integrated UVO luminosity in units of 10^{46} ergs s^{-1}, $r_{\rm pc}$ is the distance of the grain from the photon source in parsecs, τ is the optical depth in the UVO region, and $A_{\mu\rm m}$ is the grain size in microns. This is identical to equation (4) in Barvainis (1987) except that the grain size is explicitly included here.

For a fixed evaporation temperature $T_{\rm ev}$, the innermost distance a grain can survive is

$$r_{\rm in} = 9 \times 10^8 T_{\rm ev}^{-2.8} [0.05/A_{\mu\rm m}]^{1/2} L_{\rm UVO,46}^{1/2} e^{-\tau/2} \text{ pc} . \quad (2)$$

For $L_{\rm UVO,46} \sim 0.6$ (typical for GQ Com in a high state), $A \sim 0.15$ μm, and $T_{\rm ev} \sim 1700$ K, $r_{\rm in} \sim 0.3$ pc. Therefore, we expect the hottest grains to respond to changes in the UVO flux with a delay of about 1 yr, unless they are situated near the line of sight.

In our model, the dusty disk sees the radiation of a more highly inclined accretion disk than does the observer. In accretion disks around rapidly rotating black holes, the observed integrated flux is nearly independent of the inclination angle; only the spectral hardness (mean observed temperature) is affected. The lowermost curve and uppermost curves in Figure 1 show the result of assuming a zero response time for the IR-emitting region. It is apparent that a zero delay in the IR response to the rising UV flux greatly overpredicts the 2 μm emission. The curve that crosses over between the upper UV and lower IR curves shows the result of including the time delay predicted on the basis of the model which has an inner dusty disk edge of a few hundred light-days.

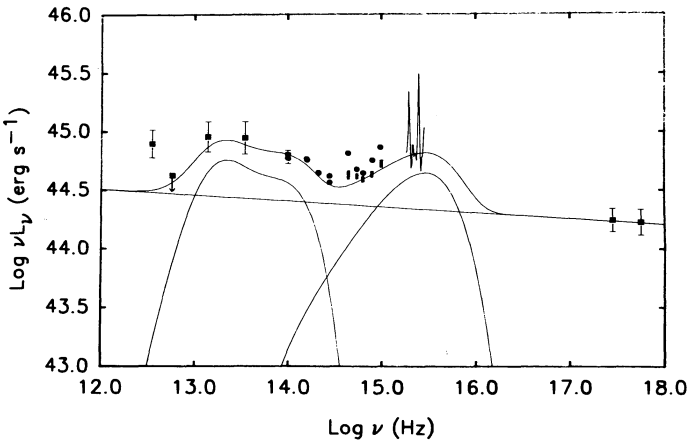

FIG. 7.—The energy distribution of GQ Com in 1986 February, and the model fit to the data. The higher frequency component is the emission from the accretion disk. The lower frequency component is the emission by the dust heated by the accretion disk radiation. The straight line is a power law indicating the maximum emission allowed due to other processes and is required in this model to explain the observed 1 μm emission and the X-ray flux.

Figure 7 shows the fit to the data from 1986 February 14 and also shows the contributions of the three continuum components. The IR emission was determined as follows. For simplicity, the disk was divided into three concentric toroidal sections, with mean delays of 250 days (equal to the observed 2 μm delay time discussed in § 3), 3–5 yr, and a *steady* outer region that dominates the far-IR emission, powered by the disk flux emitted more than 5 yr earlier. These correspond to sections with $r \leq 0.5$ pc, 0.5 pc $\leq r \leq 1.5$ pc, and $r \geq 1.5$ pc. The heights of the inner tori are comparable to their mean radii for the opening angle assumed, and for this rough illustration, the additional effects of the dusk disk thickness on the response time was ignored (i.e., the vertical thicknesses of the two inner toroids are the same as their horizontal thicknesses, to first order, and the disk is face-on). The heating was determined by integrating the energy for $\lambda < 1$ μm due to the accretion disk and the power law for the best-fit model to the "Big Blue Bump" for each epoch. The continuum was defined by the *IUE* spectrum in the UV, and the *V* (0.55 μm) band in the optical. The emission from the inner region is due to heating by the *UVO* flux observed around 1985 May modeled with an accretion rate of 0.15 $M_\odot$ yr^{-1}. For the middle section, the mean flux from 1981 February through 1984 (determined from six observations using the photometry data in Table 2), which gives a mean accretion rate of 0.08 $M_\odot$ yr^{-1}. For the outer region, which dominates the far-IR emission, the historical value of the mean visual flux was used to estimate a historical mean accretion of 0.12 $M_\odot$ yr.

The data show that the UVOIR data of GQ Com, and presumably AGNs in general, can be explained quite naturally as the result of direct radiation of an accretion disk, and reradiation of a dusty disk. Both the spectral shape and variability time scale are consistent with this hypothesis. In this model, $L_{IR} \sim 0.6 L_{UVO}$. This is less than the value of $0.8 L_{UVO}$ expected if the disk were optically thick to the UVO radiation along all lines of sight. As mentioned earlier, however, much of the disk in this model has τ between 1 and 2, allowing some of the primary radiation through. For $\tau = 1.5$, 22% of the radiation is unabsorbed as it traverses the dust disk.

5. DISCUSSION

5.1. *Accretion Disk Variability*

As shown in Figure 1, very adequate fits to the changes in the UVO luminosity of GQ Com can be made simply by changing one parameter—the accretion rate. For all 11 epochs of the data between 1984 November and 1986 May, the data are well-represented using a disk of inclination cos $i = 0.75$, accreting onto a maximally rotating black hole of mass $3 \times 10^8 M_\odot$, and by changing the accretion rate between 0.042 $M_\odot$ yr^{-1} (1985 February) and 0.15 $M_\odot$ yr^{-1} (1985 May). These values are consistent with those of Sun & Malkan (1989), who use a similar accretion disk model, but different "additional" emission components (modeling a single "snapshot" of GQ Com they get a mass of $5 \times 10^8 M_\odot$ yr^{-1} and an accretion rate of 0.08 $M_\odot$ yr^{-1} for cos $i = 0.75$). These values are also within the 90% confidence limits for the fits that Laor (1990) has made to the same object, using an accretion disk model that includes radiative transfer effects within the disk atmosphere, and a simple power law (these confidence limits are, however, extremely large).

However, viscous time scales on which accretion rates can change from one steady state to another are far too long ($\sim 10^4$–10^5 yr) to explain the observed variability. Therefore, another mechanism is required to globally change the heating of the disk in such a way as to crudely mimic a variable accretion rate. The mechanism requires that all portions of the disk can respond very quickly to the initial outburst, yet allow the cooler, more distant regions to relax more slowly (since the decline in the *V* band is slower than that in the UV).

Two possible mechanisms can achieve a more rapid response time for global changes in the disk. First, scattering of accretion disk radiation by a cloud of material above the disk plane (such as a corona) can heat the whole disk in response to an increase in flux from any portion of it. Second, a concave disk can heat itself directly, as all parts of the disk have unobstructed views of the other parts.

5.2. *Dust Emission Variability*

The preliminary version of this model gives a very reasonable fit to most of the IR spectrum and has a large UV-to-IR time delay. It is thus consistent with the hypothesis that the IR emission is due to dust grains heated by the UV radiation of the central source. However, the fit is not a perfect one, in that to fit the near-IR flux it was necessary to have the inner edge of the dust disk 0.3 pc (360 lt-days) from the central source, with a mean IR delay nearly twice that observed. It should be possible to obtain a better fit to both the spectrum and variability simultaneously, with some adjustment of the input parameters. In particular, a proper grain size distribution, a full radiative transfer calculation (in all directions), dust disk inclination, and vertical light-travel time (ignored here) all need to be included. The results are also sensitive to the assumed value of T_{ev}. Furthermore, temperature excursions above the bulk evaporation temperature should be included for small grains, as Guhathakutra & Drain (1989) have shown that these grains can reach temperatures higher than expected from equilibrium calculations.

5.3. *The Third Component*

In the model outlined in this paper, the sum of the accretion disk and dust emission alone would underpredict the observed 1 μm flux and suggest another component may be present. This

may also be the reason that the variation at 1.65 μm is smaller than at 2.25 μm. Such a component must also not have significant intrinsic polarization or else the IR polarizations in normal radio-quiet quasars would be higher than are actually observed (Sitko & Zhu 1991). Optically thin free-free emission is one candidate for the source of this emission, although the source would have to be inhomogeneous to produce a ν^{-1} spectral shape suggested by the data. Far-IR emission could be Compton-scattered by a hot corona around the disk (which may also produce much of the X-ray emission). A region containing ionized gas could simultaneously produce the observed emission and provide a medium capable of polarizing both the optical and IR light by similar small amounts, as is observed. However, the Comptonization would require high Lorentz factors, and could not be due to a region gravitationally bound to the accretion disk.

6. CONCLUSIONS AND FUTURE IMPROVEMENTS

GQ Com is a highly active radio-quiet AGN which exhibits continuum and line variability on a variety of time scales. The ultraviolet continuum flux variability is characterized by a two-folding rise time of about 100 days, and a longer decline time by a factor of 3. The optical light rises simultaneously (within the time resolution of the observations), but declines more slowly. The rise in the 2.2 μm flux is delayed by nearly 250 days, while the flux at 3.5 μm responds even later. The delay times at these wavelengths is entirely consistent with their being dominated by thermal emission from dust grains heated by the central source.

We have constructed a crude model that incorporates many concepts currently under discussion in grand unified theories of AGNs. Specifically, we show that the spectral energy distribution and variability time scale in the UVOIR is consistent with a disk or torus of dust heated by a thermal accretion disk. However, a number of difficulties remain.

Regarding the central accretion disk, considerable work remains to determine the structure of the light-emitting regions and the source of the UVO variability.

For the IR, more sophisticated modeling should include: a finer dust disk size grid, a more realistic particle size distribution and composition, and a dust torus that is determined by disk hydrodynamics and the interaction of the photons from the central source with the dust grains. Pier & Krolik (1992) and Laor & Draine (1993) have begun to investigate some of these effects in greater detail.

A number of individuals deserve thanks for their help and support in the execution of the observational part of the project. These include: Bill Keel for releasing his data prior to publication; Wieslaw Wisniewski, Bob Howell, and Gary Schmidt for observing GQ Com when scheduling, instrument, or weather difficulties prevented us from getting the needed data, and Bev Wills for continued encouragement. Most of the observations were obtained while one of us (M. L. S.) was a post-doctoral fellow at Kitt Peak. This work was also supported by NASA grants NAG5-872 and NAG5-190 and the University Research Council of the University of Cincinnati (M. L. S.) and grant number 2-1188-91-01 financed by the State Committeee for Scientific Research, Poland (A. S.).

APPENDIX A

In order to help quantify the delay times seen in the light cuves, the discrete correlation function (DCF) of Edelson & Krolik (1988) was applied to the data sets. The DCF takes unevenly spaced data, performs a point-by-point correlation, and bins the data into time delay intervals that can be chosen to be evenly spaced. Errors determined from the scatter of the data in each bin can be calculated and used as a "reality check" of the significance of the resulting DCF power.

Figures 8–12 show the DCF for the UV autocorrelation and for various cross-correlations of the UV, V, H, K, and L light curves.

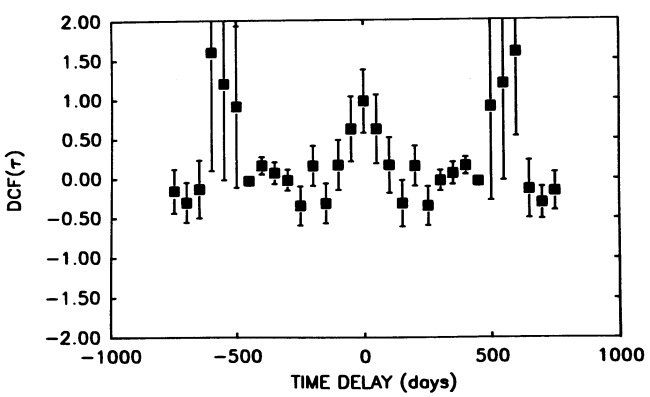

FIG. 8

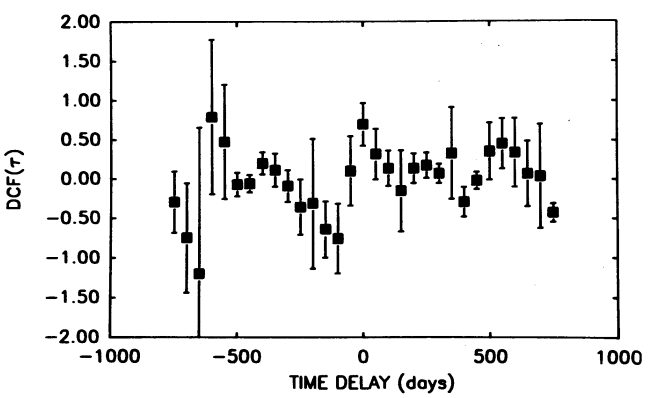

FIG. 9

FIG. 8.—The autocorrelation of the ultraviolet light curve shown in Fig. 2, using the discrete correlation function (DCF) of Edelson & Krolik (1988)
FIG. 9.—The DCF cross-correlation of the UV and V light curves of Fig. 2

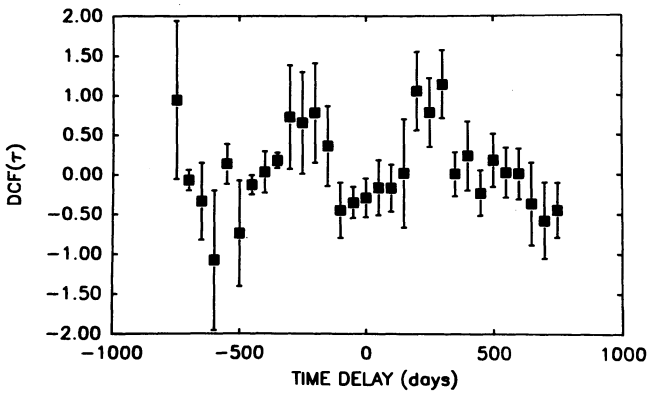

FIG. 10.—The DCF cross-correlation of the UV and *K* light curves of Fig. 3

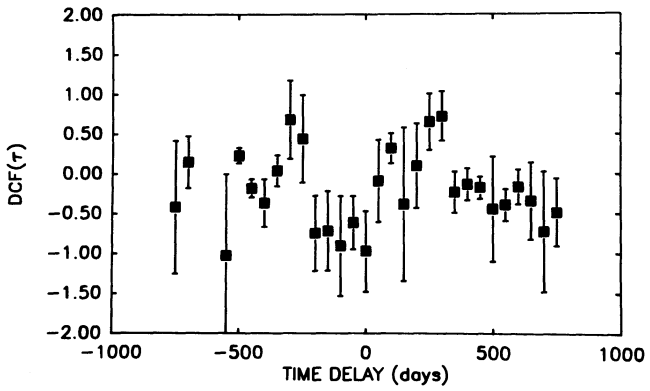

FIG. 11.—THE DCF cross-correlation of the UV and *H* light curves

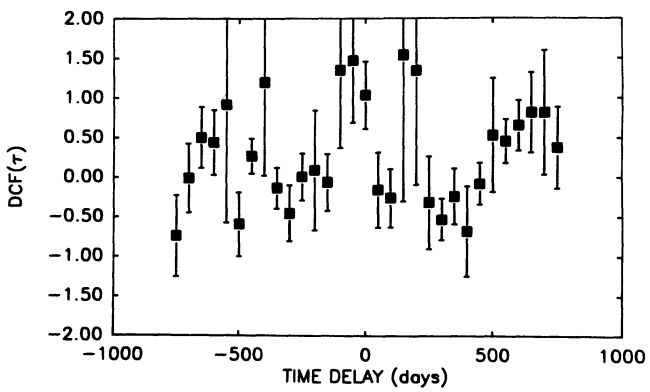

FIG. 12.—The DCF cross-correlation of the UV and *L* light curves

REFERENCES

Antonucci, R. R. J., & Miller, J. S. 1985, ApJ, 297, 621
Barvainis, R. 1987, ApJ, 320, 537
———. 1990, ApJ, 353, 419
———. 1992, ApJ, 400, 502
Bechtold, J., Czerny, B., Elvis, M., Fabbiano, G., & Green, R. F. 1986, ApJ, 314, 699
Bessell, M. S. 1976, PASP, 88, 557
———. 1979, PASP, 91, 589
Burstein, D., & Heiles, C. 1982, AJ, 87, 1165
Campins, H., Rieke, G. H., & Lebofsky, M. J. 1985, AJ, 90, 896
Cassatella, A., & Harris, A. W. 1983, NASA *IUE* Newsletter, No. 23, 21
Clavel, J., Wamsteker, W., & Glass, I. 1988, ApJ, 337, 236
Combes, F. 1991, ARA&A, 29, 195
Cunningham, C. T. 1975, ApJ, 202, 788
Czerny, B., & Elvis, M. 1987, ApJ, 321, 305
Draine, B. T., & Lee, H. M. 1984, ApJ, 285, 89
Edelson, R. A., & Krolik, J. H. 1988, ApJ, 333, 646
Edelson, R. A., & Malkan, M. A. 1986, ApJ, 308, 59
Elvis, M., Green, R. F., Bechtold, J., Schmidt, M., Neugebauer, G., Soifer, B. T., Matthews, K., & Fabbiano, G. 1986, ApJ, 310, 291
Genzel, R., & Townes, C. H. 1987, ARA&A, 25, 377
Goldreich, P., & Lynden-Bell, D. 1965, MNRAS, 130, 97
Guhathakutra, P., & Draine, B. T. 1989, ApJ, 345, 230
Hayes, D. S. 1979, Dudley Obs. Rep. No. 14, 297
Holm, A. V., Bohlin, R. C., Ponz, D. P., & Schiffer, F. H. 1982, A&A, 112, 341
Impey, C., & Neugebauer, G. 1988, AJ, 95, 307
Johnson, H. L. 1966, ARA&A, 4, 193
Landau, R., et al. 1986, ApJ, 308, 78
Laor, A. 1990, MNRAS, 246, 369
Laor, A., & Draine, B. T. 1993, ApJ, in press
Laor, A., Netzer, H., & Piran, T. 1990, MNRAS, 242, 560
Lebofsky, M. J., & Rieke, G. H. 1980, Nature, 284, 410
Malkan, M. A. 1983, ApJ, 268, 582
Massa, D., & Fitzpatrick, E. L. 1986, ApJS, 60, 305
Neugebauer, G., Graham, J. R., Soifer, B. T., & Matthews, K. 1990, AJ, 99, 1456
Novikov, I. D., & Thorne, K. S. 1973, Astrophysics of Black Holes, ed. C. DeWitt & B. S. DeWitt, (Gordon & Breach), 343
Osterbrock, D. E., & Shaw, R. A. 1988, ApJ, 327, 89
Page, D. N., & Thorne, K. S. 1974, ApJ, 191, 499
Peterson, B. M., et al. 1991, ApJ, 368, 119
Pier, E. A., & Krolik, J. H. 1992, ApJ, 401, 99
Rees, M. J., Silk, J. I., Werner, M. W., & Wickramasinghe, N. C. 1969, Nature, 223, 788
Sakimoto, P. J., & Coroniti, F. V. 1981, ApJ, 247, 19
Savage, B. D., & Mathis, J. S. 1979, ARA&A, 17, 73
Shakura, N. I., & Sunyaev, R. A. 1973, A&A, 24, 337
Simmons, J. F. L., & Stewart, B. G. 1985, A&A, 142, 100
Sitko, M. L. 1986, in Continuum Emission in Active Galactic Nuclei , ed. M. L. Sitko (Tucson: NOAO), 29
———. 1988, ApJ, 328, 170
———. 1990, ApJS, 72, 777
Sitko, M. L., Schmidt, G. D., & Stein, W. A. 1985, ApJS, 59, 323
Sitko, M. L., Stein, W. A., Zhang, Y.-X., & Wisniewski, W. Z. 1982, ApJ, 259, 486
Sitko, M. L., & Zhu, Y. 1991, ApJ, 369, 106
Stockman, H. S., Moore, R. L., & Angel, J. R. P. 1984, ApJ, 279, 485
Stoughton, R., & Osterbrock, D. E. 1980, PASP, 92, 117
Sun, W.-H., & Malkan, M. A. 1989, ApJ, 346, 68
Tran, H. D., Miller, J. S., & Kay, L. E. 1992, ApJ, 397, 452
Zheng, W., Burbidge, E. M., Smith, H. E., Cohen, R. D., & Bradley, S. E. 1987, ApJ, 322, 164